Radiation Physics and Chemistry xxx (xxxx) xxx–xxx

Contents lists available at ScienceDirect

Radiation Physics and Chemistry

journal homepage: www.elsevier.com/locate/radphyschem

X-ray and optical characterization of the intermediate products in the Au^{3+} reduction process by oleylamine

Mikhail V. Kirichkov[a], Alexander A. Guda[a,*], Andriy P. Budnyk[a], Aram L. Bugaev[a], Tatiana A. Lastovina[a], Victor V. Shapovalov[a], Sergey A. Guda[a,b], Alexander L. Trigub[c,d], Yuri V. Rusalev[a], Anatoly V. Chernyshev[e], Carlo Lamberti[a,f], Alexander V. Soldatov[a]

[a] The Smart Materials Research Institute, Southern Federal University, 344090 Rostov-on-Don, Russia
[b] Institute of Mathematics, Mechanics and Computer Science, Southern Federal University, 344090 Rostov-on-Don, Russia
[c] National Research Centre "Kurchatov Institute", 123098 Moscow, Russia
[d] Institute of Geology of Ore Deposits (IGEM RAS), 119017 Moscow, Russia
[e] Institute of Physical and Organic Chemistry, Southern Federal University, 344090 Rostov-on-Don, Russia
[f] Department of Physics, CrisDi and NIS Interdepartmental Centres and INSTM Reference Center, University of Turin, via Pietro Giuria 1, 10125 Turin, Italy

ARTICLE INFO

Keywords:
Colloidal gold
XANES
EXAFS
UV-vis
DLS
Oleylamine

ABSTRACT

Formation of gold nanoparticles (NPs) from the mixture containing $NaAuCl_4$ as a precursor, octadecene as a solvent and oleylamine as a reducing agent was studied *in situ* by means of optical and X-ray spectroscopies. Dynamic light scattering (DLS) revealed the presence of initial aggregates of 500 nm average size which split into nanoparticles of about 8 nm width shortly after the reduction from Au^{3+} to Au^{+} has been completed. Based on Density Functional Theory (DFT) simulations and analysis of X-ray absorption spectra (XAS) we identified the structure of Au^{3+} and Au^{+} gold complexes. Quantitative analysis shows that Au NPs formation proceeds in following steps: substitution of chlorine ligands in Au^{3+} complex by four oleylamines; reduction of Au^{3+} to Au^{+} coordinated by two oleylamines. Latter process occurs in oleylamine micelles in octadecene. The third step is a fragmentation of large micelles into smaller ones shortly after reduction Au^{3+} to Au^{+}, and subsequent slow growth of Au NPs via reduction of Au^{+} to Au^{0}.

1. Introduction

Au NPs find applications in biomedicine, catalysis and electronics due to a unique combination of size effects, active surface atoms and high electron conductivity (Corma and Garcia, 2008; Jain, 2014). Knowledge about elementary steps of the gold ion reduction is important for tuning the size and shape of resulting NPs during synthesis. Oleylamine's (OAm) amino group can act as an electron donor upon increasing temperature, while its long hydrocarbon chain allows to stabilize the resulting NPs (Aslam et al., 2004; Huo et al., 2008). Its hydrophilic and hydrophobic parts form micelles which act as microreactors for the nucleation and growth of NPs (Liu et al., 2007; Kosmella and Koetz, 2006). *In situ* investigation of the gold reduction in such micelles is crucial for the understanding of the speciation of intermediates and kinetics of the process. XAS has not yet been applied for the characterization of gold reduction by OAm; existing examples of the *in situ* characterization concern Au^{3+} reduction in water by citrate or citric acid (Mikhlin et al., 2011; Polte et al., 2010a,b; Yao et al., 2010). In the presence of PVP stabilizer (Yao et al., 2010) combined XANES and EXAFS analysis predicts partial reduction from $AuCl_4^-$ to $AuCl_3^-$ and subsequent formation of dimers and bigger Au_nCl_{n+x} clusters rather than Au_n^0 clusters. XANES and SAXS did not provide experimental evidence for the existence of intermediate Au^{+} stage in the citrate or sodium borohydride reduction process (Polte et al., 2010a,b).

The goal of our present work is to use a combination of X-ray and optical methods to characterize intermediate states of gold in the process of Au^{3+} reduction by OAm in octadecene.

2. Methods

Synthesis of Au NP was performed by method described in (Wang et al., 2012). 2 ml of OAm, 0.1 g of $NaAuCl_4$ and 20 ml of 1-octadecene (Sigma Aldrich) were mixed at room temperature, heated up to 80 °C and left over 120 min. UV-vis spectra were measured *in situ* with a Shimadzu UV-2600 spectrometer in a 10 mm quartz cell. DLS was

* Corresponding author.
E-mail address: guda@sfedu.ru (A.A. Guda).

https://doi.org/10.1016/j.radphyschem.2018.11.021
Received 30 September 2018; Received in revised form 21 November 2018; Accepted 23 November 2018

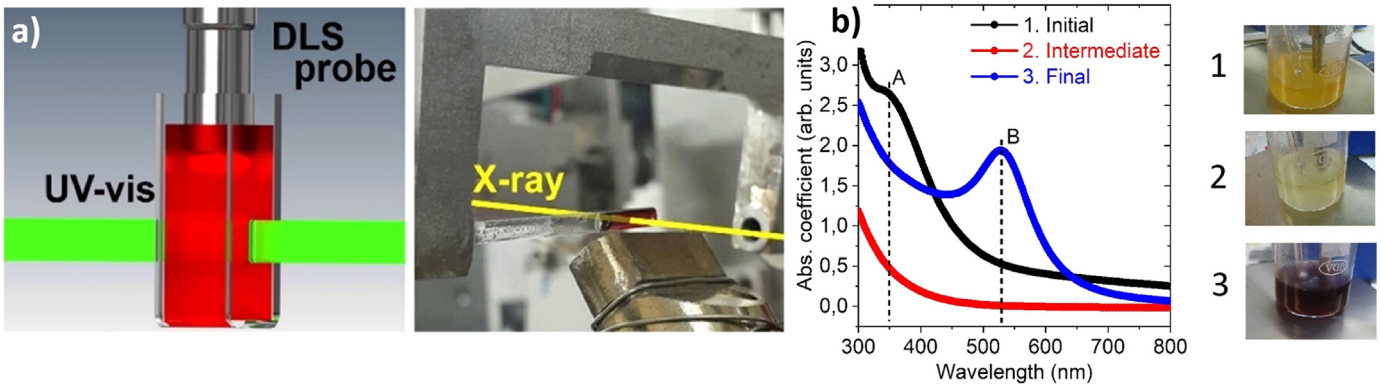

Fig. 1. (a) Scheme of the experimental setup for the combined UV-vis and DLS (*left side*) and XAS (*right side*) measurements and (b) the main stages of the synthesis of Au NPs according to UV-vis analysis.

measured through the optical fiber of a Microtrac Nano-flex simultaneously with acquisition of UV-vis spectra. Both XANES and EXAFS were measured at the BM01b beamline (successively moved to the BM31 port) of ESRF (Grenoble, France) and at the beamline "Structural Materials Science" (Mozhchil et al., 2015) of Kurchatov Synchrotron Radiation Source (Moscow, Russia). Spectra were measured in the transmission mode with Si(111) monochromator. Gold foil was placed between the second and the third ionization chambers for spectra energy calibration. Experimental scheme is shown in Fig. 1a.

3. Results and discussion

The characteristic color of the Au^{3+} water solution is yellow, which is due to characteristic absorption of the $[AuCl_4]^-$ complex at 313 nm. The rise of absorption band at 350 nm in the beginning of synthesis (peak A in Fig. 1b) indicates formation of the Au^{3+} complex, whose chlorine ligands are substituted with amino groups.

Then color of the reaction mixture during the first hour of reaction changes from the orange to the colorless and later within the next hour to deep red. Red color appears due to surface plasmon resonance (SPR) of Au NPs (peak B at 535 nm in Fig. 1b, see also Fig. S1 in SI). The amplitude of the SPR peak can be used to quantify the size of Au NPs as reported in Haiss et al. (2007). The Au NPs diameter, calculated from the ratio of absorbances at 535 nm (SPR) and at 450 nm (reference point), increases over time of reaction, as shown in Fig. 2a. The growth of Au NPs in OAm is slow in contrast to the fast nucleation and growth in a classical Turkevich synthesis (Turkevich et al., 1951). It evidently begins after 60 min of the reaction and finishes after 120 min.

DLS data were acquired simultaneously with UV-vis spectra. Fig. 2b presents size distributions for scattering particles as a function of time. At the beginning of synthesis, the reaction mixture contains agglomerates with an average size of 500 nm. They originate from reverse micelle-like structures formed by OAm (Wang et al., 2007) confining the Au^{3+} complexes. Large OAm micelles release small nuclei of gold after 70 min of the reaction. These nuclei are covered by a shell of OAm which is consistent with a model provided in the work (Yao et al., 2010), where PVP was used as a stabilizer.

After the initial reaction mixture had been rapidly heated to 80 °C the Au L_3 XANES were measured every 3 min (Fig. 2c). The intensity of the white line at 11,920 eV decreases over the first 20 min of the reaction, indicating reduction of the Au^{3+} to Au^{+}. The spectrum of the intermediate component (red one in Fig. 2c) is similar to that of $[AuCl_2]^-$ reported in Pokrovski et al. (2009) and Chang et al. (2015) as well as to the spectrum of Au(tht)Cl shown in Helmbrecht et al. (2015), allowing attribution to the Au^+ complex with OAm (Huo et al., 2008). PCA analysis (Guda et al., 2019) performed for the series of data (see SI for the details) indicated absence of additional components, e.g. Au^{2+} species, observed in situ recently by Szlachetko et al. (2014) during the temperature-programmed reduction of Au_2O_3.

At the end of the reaction Au L_3 XANES indicate formation of small Au NPs (blue line in Fig. 2c). The EXAFS analysis (Fig. 3a and Section 3 in SI) performed for the Au^{3+} and Au^+ intermediate species according to Zabinsky et al. (1995), evidences the changes in coordination number in the first coordination shell of gold. Initial Au^{3+} is coordinated by 4 nitrogen atoms, and upon transition to Au^+, the coordination number is reduced to 2.

Results of EXAFS fit are further supported by DFT calculations at B3LYP level of theory (ADF-2017 program package, QZ4P basis set (Fonseca Guerra et al., 1998). DFT results predict the Au-Cl distance to be larger than 2.3 Å for both the Au^{3+} and Au^+ complexes. However, experimentally found distances in the first coordination shell were less than 2.05 Å. Therefore, we can exclude Cl atoms from the first coordination shell and conclude that when $NaAuCl_4$ is dissolved in OAm, the Cl ligands are substituted by OAm molecules. The XANES spectra,

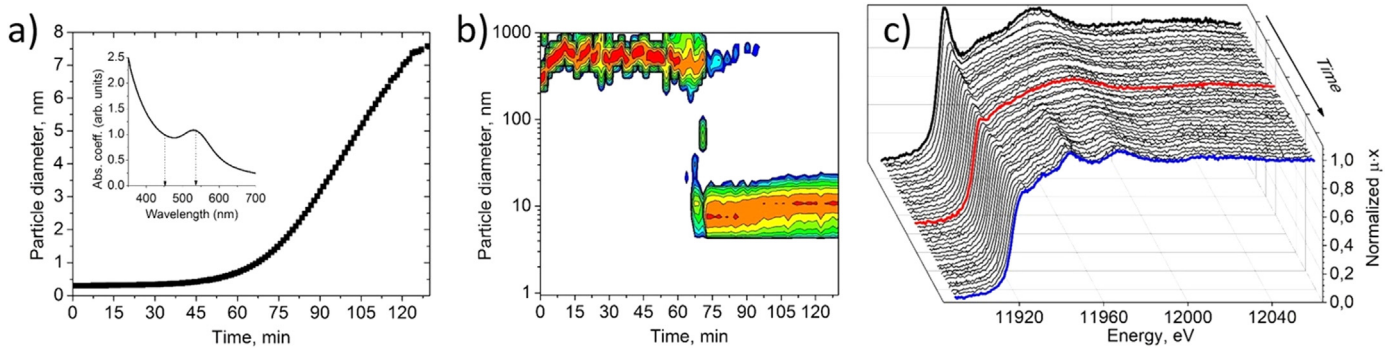

Fig. 2. (a) Quantification of the size of Au NPs from the UV-vis data as a function of reaction time, (b) particle size distribution obtained from experimental DLS data measured in situ during formation of GNPs, (c) *in situ* Au L_3 XANES of the reaction mixture at 80 °C measured every 3 min.

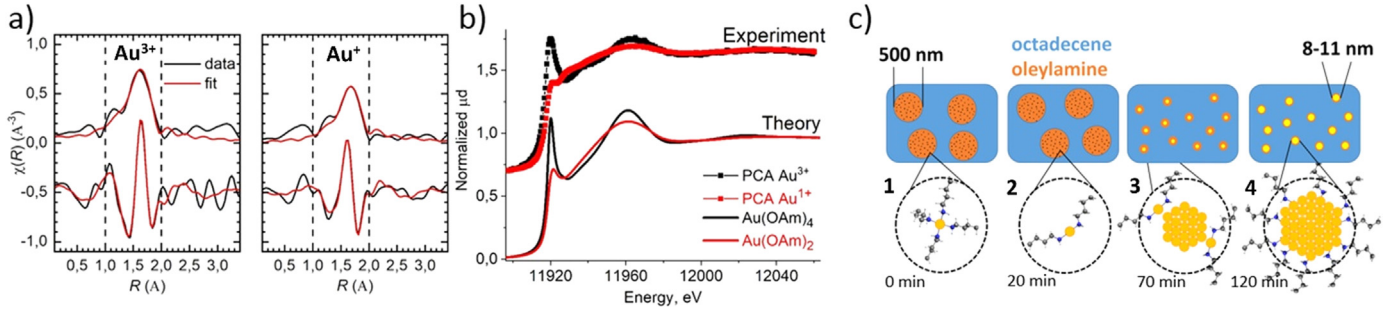

Fig. 3. (a) Amplitudes and imaginary parts of experimental (solid black lines) and fitted (solid red lines) k^2-weighted Fourier-transforms of EXAFS spectra of Au^{3+} and Au^{+}. (b) comparison between experimental Au^{+}, Au^{3+} PCA components obtained for Au L_3 XANES in the reaction in OAm/octadecene solution and theoretical simulation for the $[Au(OAm)_4]^{3+}$ and $[Au(OAm)_2]^{+}$ structures, obtained from DFT, (c) scheme of the stages of the reaction.

calculated with the finite difference approach within FDMNES software (Guda et al., 2015) for the DFT relaxed structures of $[Au(OAm)_4]^{3+}$ and $[Au(OAm)_2]^{+}$, (bottom spectra in Fig. 3b and Section 4 in SI) are in a good agreement with experimental ones (top spectra).

Fig. 3c schematically combines the conclusions derived from optical and X-ray characterization. Initial $[Au(OAm)_4]^{3+}$ complexes are coordinated by four OAm molecules and form micelles of hundreds nm size (1 in Fig. 3c). Upon reduction to Au^{+} number of coordinated OAm molecules is reduced to two (2 in Fig. 3c). After 60 min small gold clusters are formed upon reduction of some Au^{+} ions to Au^{0}. They get released then from the micelle remaining surrounded by the OAm shell (3 in Fig. 3c). The final stage is the growth of Au NPs until ~11 nm size until full depletion of Au^{+} precursor (4 in Fig. 3c). Our results show that gold reduction in octadecene proceeds in dense droplets of OAm as in 'nano-reactors' – the similar concept has been already suggested for citrate synthesis (Mikhlin et al., 2011; Kumar et al., 2007). Due to generally slower kinetics of the process, we were able to register experimentally and to characterize Au^{+} intermediate state while for the fast citrate reduction this step is still remains poorly studied.

4. Conclusions

We performed XAS and UV-vis *in situ* characterizations of Au NPs growth in octadecene medium upon $NaAuCl_4$ reduction by OAm. DLS revealed that initial agglomerates of about 500 nm are split into small 8 nm particles after 70 min of the reaction at 80 °C. It occurs after reduction of all Au^{3+} ions into Au^{+} and partial reduction of Au^{+} into Au^{0}. Initial and intermediate species were identified by theoretical analysis of the Au L_3 XAS spectra. We found that initial Au^{3+} complex was coordinated by four N located at 2.04 Å and Au^{+} complex is coordinated by two N atoms at 2.05 Å. We, thus, exclude the presence of chlorine atoms in the first coordination of gold ions at all stages of nanoparticle formation.

Acknowledgments

AAG, ALB, AVS acknowledge the Grant of the Southern Federal University (VnGr-07/2017-08) for the financial support.

Appendix A. Supporting information

Supplementary data associated with this article can be found in the online version at doi:10.1016/j.radphyschem.2018.11.021.

References

Aslam, M., Fu, L., Su, M., et al., 2004. J. Mater. Chem. 14, 1795–1797. https://doi.org/10.1039/B402823F.
Chang, S.-Y., Uehara, A., Booth, S.G., et al., 2015. RSC Adv. 5, 6912–6918. https://doi.org/10.1039/C4RA13087A.
Corma, A., Garcia, H., 2008. Chem. Soc. Rev. 37, 2096–2126. https://doi.org/10.1039/B707314N.
Fonseca Guerra, C., Snijders, J.G., te Velde, G., et al., 1998. Theor. Chem. Acc. 99, 391–403. https://doi.org/10.1007/s002140050353.
Guda, S.A., Guda, A.A., Soldatov, M.A., et al., 2015. J. Chem. Theory Comput. 11, 4512–4521. https://doi.org/10.1021/acs.jctc.5b00327.
Guda, A.A., Guda, S.A., Lomachenko, K.A., Soldatov, M.A., Pankin, I.A., Soldatov, A.V., Braglia, L., Bugaev, A.L., Martini, A., Signorile, M., Groppo, E., Piovano, A., Borfecchia, E., Lamberti, C., 2019. Quantitative structural determination of active sites from in situ and operando XANES spectra: from standard ab initio simulations to chemometric and machine learning approaches. Catal. Today. https://doi.org/10.1016/j.cattod.2018.10.071. (in press).
Haiss, W., Thanh, N.T.K., Aveyard, J., et al., 2007. Anal. Chem. 79, 4215–4221. https://doi.org/10.1021/ac0702084.
Helmbrecht, C., Lutzenkirchen-Hecht, D., Frank, W., 2015. Nanoscale 7, 4978–4983. https://doi.org/10.1039/C4NR07051H.
Huo, Z., Tsung, C.-k., Huang, W., et al., 2008. Nano Lett. 8, 2041–2044. https://doi.org/10.1021/nl8013549.
Jain, P.K., 2014. Angew. Chem. Int. Ed. Engl. 53. https://doi.org/10.1002/anie.201309807.
Kosmella, S., Koetz, J., 2006. Colloids Surf. A Physicochem. Eng. Asp. 290, 150–156. https://doi.org/10.1016/j.colsurfa.2006.05.018.
Kumar, S., Gandhi, K.S., Kumar, R., 2007. Ind. Eng. Chem. Res. 46, 3128–3136. https://doi.org/10.1021/ie060672j.
Liu, X., Atwater, M., Wang, J., et al., 2007. J. Nanosci. Nanotechnol. 7, 3126–3133. https://doi.org/10.1166/jnn.2007.805.
Mikhlin, Y., Karacharov, A., Likhatski, M., et al., 2011. J. Colloid Interface Sci. 362, 330–336. https://doi.org/10.1016/j.jcis.2011.06.077.
Mozhchil, R.N., Menushenkov, A.P., Ionov, A.M., et al., 2015. Phys. Procedia 71, 318–322. https://doi.org/10.1016/j.phpro.2015.08.337.
Pokrovski, G.S., Tagirov, B.R., Schott, J., et al., 2009. Chem. Geol. 259, 17–29. https://doi.org/10.1016/j.chemgeo.2008.09.007.
Polte, J., Ahner, T.T., Delissen, F., et al., 2010a. J. Am. Chem. Soc. 132, 1296–1301. https://doi.org/10.1021/ja906506j.
Polte, J., Erler, R., Thünemann, A.F., et al., 2010b. ACS Nano 4, 1076–1082. https://doi.org/10.1021/nn901499c.
Szlachetko, J., Sá, J., Nachtegaal, M., et al., 2014. J. Phys. Chem. 80–84. https://doi.org/10.1021/jz402309s.
Turkevich, J., Stevenson, P.C., Hillier, J., 1951. Discuss. Faraday Soc. 11, 55–75. https://doi.org/10.1039/DF9511100055.
Wang, C., Hou, Y., Kim, J., et al., 2007. Angew. Chem. Int. Ed. Engl. 46, 6333–6335. https://doi.org/10.1002/anie.200702001.
Wang, M., Wang, C., Young, K.L., et al., 2012. Chem. Mater. 24, 2423–2425. https://doi.org/10.1021/cm300381f.
Yao, T., Sun, Z.H., Li, Y.Y., et al., 2010. J. Am. Chem. Soc. 132, 7696–7701. https://doi.org/10.1021/ja101101d.
Zabinsky, S.I., Rehr, J.J., Ankudinov, A., et al., 1995. Phys. Rev. B 52, 2995–3009. https://doi.org/10.1103/PhysRevB.52.2995.